Materials Science-Poland
Volume 43 Issue 3 · pp. 124–145 · DOI: 10.2478/msp-2025-0034

Materials Science-Poland

Experimental accuracy verification of the common practice analysis of doubly reinforced shallow concrete beams reinforced by steel grade 500

Research Article

Hassan M. Magbool*, Ahmed A. El-Abbasy

Civil and Architectural Engineering Department, College of Engineering and Computer Science, Jazan University, Jazan, Saudi Arabia

Received 07 August 2025; Accepted 06 October 2025

Abstract: Beam designers typically use only tension reinforcement. A beam's moment strength can be increased either by increasing the tension reinforcement area or by increasing the beam depth. However, when architectural or functional constraints limit the beam's cross-section, a compression reinforcement is added to enhance moment strength. This study aims to assess the validity of the accuracy analysis and design methods for doubly reinforced sections as suggested by various provisions and codes. The study conducted an experimental investigation involving three beams, each with a compression steel to tension steel ratio of 0.2, 0.3, and 1. Furthermore, this study aims to develop a proposed analytical method for the design of doubly reinforced shallow beams utilizing grade 500 steel. The experimental results showed that all beams failed at a compression strain in concrete approximately equal to 0.0015, which is almost one-half of that recommended in most codes. It was clear that using steel grade 500 in doubly reinforced beams of shallow depths requires a high percentage of compression reinforcement to avoid compression-controlled failure, which is uneconomic compared with increasing concrete dimensions. The conventional analysis of such sections is not reasonable; therefore, the proposed analytical method effectively predicted the experimental values of the ultimate load and maximum bending moment of the beam with acceptable accuracy, exhibiting an error of approximately 11%.

Keywords: *Doubly reinforced section • Concrete • Compression steel • Grade 500 steel • Compression-controlled failure • Strain • Shallow beam*

1. Introduction

The variation in regulatory building provisions across different countries presents a significant challenge, particularly in adapting to these differences, which poses an additional hurdle for engineers. The building codes vary in terms of design equations, safety factors for materials, load considerations, etc. Understanding the key characteristics and distinctions among different building codes of practice is considered essential for establishing consistent guidelines worldwide. The concrete may not be able to achieve the necessary compression force to resist the specified bending moment if the beam cross-section is restricted due to architectural or other considerations. By adding reinforcement in the compression zone, a doubly reinforced beam is formed, which has both compression and tension reinforcement [1,2]. Figure 1 illustrates the stress and strain distributions of a doubly reinforced rectangular beam, utilizing the simplified stress block, as outlined in ACI 318 [3]. The application of strength design approaches that consider the entire strength capacity of the concrete on the compressive side has led to a significant decrease in the use of compression reinforcement. Space or aesthetic limitations may necessitate the use of beams with small dimensions, which in turn requires the inclusion of compression steel alongside tensile steel reinforcement [4,5]. The moment capacity of a beam with a maximum reinforcement ratio can be enhanced by incorporating reinforcement in both the tensile and compression zones, particularly when ε_t = 0.005. Compressive steel enhances the beam's curvature, allowing it to withstand greater loads before total failure,

* *E-mail: h.magbool@jazanu.edu.sa*

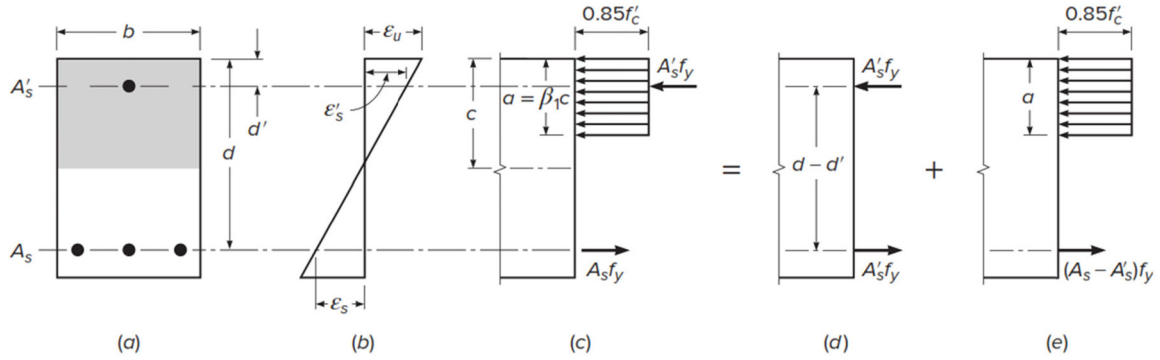

Figure 1. Analysis of a doubly reinforced rectangular beam [9]. (a) Cross-section, (b) Strain distribution, (c) Stress and forces, (d) Forces from Part 1, and (e) Forces from Part 2.

thereby increasing its ductility. The incorporation of compression steel reinforcement enhances the toughness and ductility of beams, allowing them to withstand greater bending moments, stress reversals, and deformations that may arise during seismic events [6,7]. Numerous earthquake codes require that a specific minimum amount of compression steel reinforcement be incorporated into flexural members [8].

High-strength reinforcing steel had a characteristic yield strength of 500 MPa. This designation indicates that the steel has a minimum yield strength of 500 N/mm² under standard testing conditions. Grade 500 steel represents a higher strength classification compared to conventional reinforcing steel grades (such as Grade 240, Grade 360, or Grade 420), allowing for reduced cross-sectional areas of reinforcement while maintaining equivalent load-carrying capacity. The higher strength grade enables more economical designs and is particularly beneficial in high-rise construction and heavily loaded structural members where reinforcement congestion might otherwise be problematic. High-strength steel has been developed as a result of advancements in steel production, enabling the construction of thinner and more effective structural members. However, the behavior of such elements, especially shallow beams, requires further investigation to ensure their performance under various loading conditions [10,11]. The shallow beams can be defined as the structural members characterized by a span-to-depth ratio typically greater than 2.5–3.0, where the beam's length significantly exceeds its cross-sectional depth. In shallow beams, plane sections remain approximately plane after bending (Bernoulli–Euler beam theory applies), and failure is generally governed by flexural behavior rather than shear. These beams exhibit linear strain distribution across their depth and are commonly found in typical building construction where architectural constraints limit beam depth. While the current design code (e.g., ACI 318 and EC 2) provides provisions for doubly reinforced shallow concrete beams, its adequacy with high-strength steel, such as grade 500 MPa and more, is inadequately verified. These codes were mainly developed and valid for members with normal-strength reinforcement. As a result, they may fail to make accurate predictions of the flexural capacity and failure mode of doubly reinforced shallow concrete beams, as they do not fully account for the beam failing before the maximum strain in the concrete on the compression side (0.003) associated with the high steel strength. This difference in code provisions requires targeted research to develop more reliable and efficient design models for this specific class of structural members. The primary possible failure of direct code application is threefold: (i) excessive crack width under service load – high-strength steel under service load at the same load level leads to proportionally wider flexural cracks compared to normal-strength steel. While codes such as ACI 318 provide cracked control equations, they are empirically derived from a database of beams with normal-strength steel. Their accuracy and safety when applied to beams made of high-strength steel, especially shallow beams where crack control is more critical, have not yet been fully verified. This can lead to non-compliance with states despite sufficient final strength, (ii) Deflection control – shallow beams are naturally susceptible to large deflection. The use of high-strength steel, with its highly acceptable stress, often results in small reinforcement areas (AS) for the same moment capacity. This reduces the stiffness of the section (effective moment of inertia, IE), possibly leading to deflections exceeding code-based boundaries, even if the needs of strength are satisfied. (iii) Ductility and minimum reinforcement requirements – code provisions for minimal flexural reinforcement (AS, min) are designed to ensure a ductile

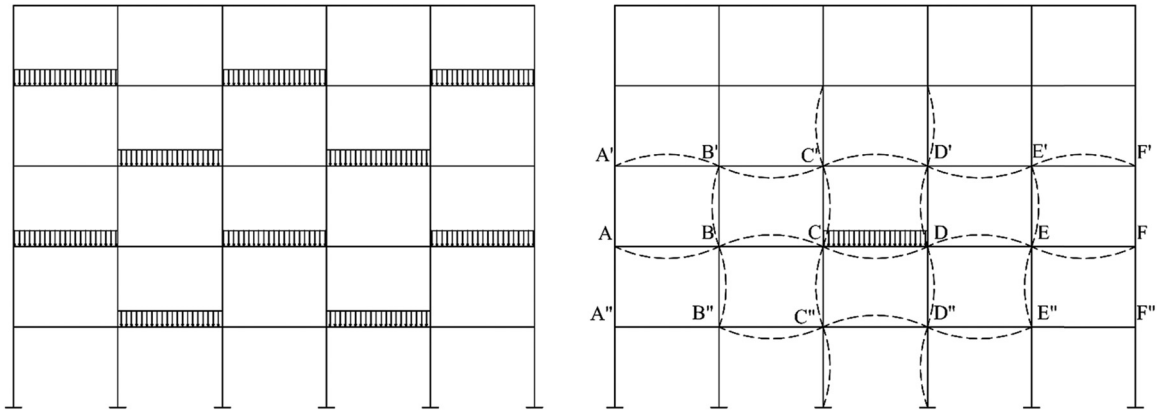

Figure 2. Alternate live loadings for minimum and maximum effects.

failure mode by giving steel yield before concrete crushing. These equations are a function of steel yield power (Fy). For high-strength steel, as min becomes quite small. In shallow beams, this minimum amount of steel may be insufficient to prevent a brittle failure or to control the cracks sufficiently, leading to a conflict between strength and serviceability design objectives.

In addition to strength, compressive reinforcement can be used for other reasons. The inclusion of compression steel has been observed as a factor in reducing the long-term deflections of flexural members. In certain instances, reinforcement bars will be positioned within the compression zone to accommodate minimal-moment loading conditions. Figure 2 illustrates an instance of the live load arrangement in the reinforced concrete frames. The objective of arranging live loads on reinforced concrete continuous beams is to identify the most important loading configurations that yield the maximum bending moments. The application of live load on some reinforced concrete beam spans generates negative moments in the unloaded spans, requiring the incorporation of steel in the compression zone to resist these moments.

The compression zone will include bars as stirrup hangers that will remain throughout the beam span (as shown in Figure 3). When the longitudinal bars are cut off along the beam's length due to reduced requirements for bending moment strength, a portion of the longitudinal bar must extend along the beam to function as stirrup hangers. Generally, building codes specify the required number of bars that must remain intact. The bars serving as stirrup hangers, typically located within the compression zone, are essential for the effective operation of shear reinforcement and the overall structural integrity of the reinforced concrete beam. They represent a crucial aspect in the realm of reinforced concrete construction. Although compression reinforcement is often neglected in flexural calculations, it may still be a good idea to take into account the presence of such reinforcement in flexural design. Therefore, this article aims to assess the validity of the accuracy analysis and design methods for doubly reinforced sections as suggested by various provisions and codes. The study conducted an experimental investigation that involved three beams, each with a compression steel to tension steel ratio of 0.2, 0.3, and 1. Furthermore, this study aims to develop a proposed analytical method for the design of doubly reinforced shallow beams utilizing grade 500 steel.

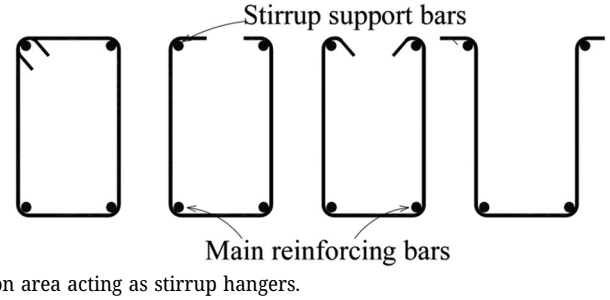

Figure 3. Bars in the compression area acting as stirrup hangers.

2. Theoretical analysis of doubly reinforced concrete sections

The rectangular cross-sections provided with both compression and tension steel reinforcement to resist bending moments are typically illustrated in code provisions and their manuals [3,12–15]. Many textbooks explain how to design these doubly reinforced concrete flexural members [9,16–21]. Also, several researchers deal with the analysis and design of such sections [8,22–26]. This analysis is, briefly, reviewed in the following sections.

2.1 Tension and compression steels are both subject to yield stresses

Regarding a doubly reinforced beam, if the tensile reinforcement ratio (ρ) is either below or equal to the balanced reinforcement ratio (ρ_b) by disregarding the compression bars, it is possible to approximate the strength of the doubly reinforced beam within acceptable levels. Tensile yielding is responsible for controlling the strength of this beam, and the presence of the compression bars will usually not have a significant impact on the lever arm of the resisting moment. A more detailed analysis is necessary if $\rho > \rho_b$. The cross-section of a rectangular beam in Figure 1(a) shows compression steel A_s' being positioned at a distance d' from the compression face, while tensile steel A_s is located at an effective depth d. The initial assumption is that both A_s' and A_s are stressed to f_y at failure. Two components can be used to calculate the total resisting moment. Figure 1(d) illustrates the coupling between the force in the compression steel A_s' and the force in an equal area of tensile steel, which provides the first part, M_{n1}:

$$M_{n1} = A_s' f_y (d - d'). \tag{1}$$

As shown in Figure 1(e), the remaining tension steel $A_s - A_s'$ acting with the compression concrete contributes to the second part, M_{n2}:

$$M_{n2} = (A_s - A_s') f_y \left(d - \frac{a}{2}\right), \tag{2}$$

where a, the depth of the stress block, is given as

$$a = \frac{(A_s - A_s') f_y}{0.85 f_c' b}. \tag{3}$$

This can be rewritten using the definitions of $\rho = A_s/bd$ and $\rho' = A_s'/bd$:

$$a = \frac{(\rho - \rho') f_y d}{0.85 f_c'}. \tag{4}$$

Hence, the total nominal moment is

$$M_n = M_{n1} + M_{n2} = A_s' f_y (d - d') + (A_s - A_s') f_y \left(d - \frac{a}{2}\right). \tag{5}$$

To achieve the design strength, the nominal capacity is diminished by multiplying by the strength reduction factor $\phi = 0.90$ if the net tensile strain $\varepsilon_t < \varepsilon_{t,min}$, as specified by the safety guidelines described in the ACI Code [3]. The minimum tensile strain in the extreme tension reinforcement, $\varepsilon_{t,min}$, is defined in Figure 4.

For the reasons mentioned earlier, it is highly desirable that failure is caused by tensile yielding instead of crushing the concrete. Establishing a maximum threshold for the tensile reinforcement ratio can ensure this. Assuming the compressive steel reaches yield stress at failure, the tensile steel strain is established, which is equal to ε_y, as shown in Figure 1(b), to determine the

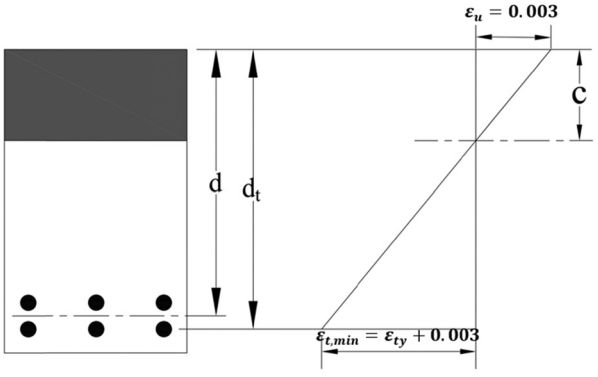

Figure 4. Minimum net tensile strain $\varepsilon_{t,min}$ for tension-controlled sections.

position of the neutral axis under failure situations, and then the balanced reinforcement ratio $\bar{\rho}_b$ can be evaluated by summing horizontal forces, as shown in Figure 1(c):

$$\bar{\rho}_b = \rho_b + \rho', \tag{6}$$

where ρ_b represents the balanced reinforcement steel ratio for the respective singly reinforced section that could be calculated using

$$\rho_b = 0.85\beta_1 \frac{f'_c}{f_y}\frac{c}{d} = 0.85\beta_1 \frac{f'_c}{f_y}\frac{\varepsilon_u}{\varepsilon_u + \varepsilon_y}. \tag{7}$$

The strength reduction factor ϕ is determined by the net tensile strain in the ACI Code [3] and not by the reinforcement ratio. If $\phi = 0.90$, the maximum reinforcement ratio is

$$\bar{\rho}_{max} = \rho_{max} + \rho', \tag{8}$$

where

$$\rho_{max} = 0.85\beta_1 \frac{f'_c}{f_y}\frac{\varepsilon_u}{\varepsilon_u + \varepsilon_{t,min}}. \tag{9}$$

If $\rho \le \bar{\rho}_{max}$, there is no need to check if ε_t is required to ascertain ϕ because $\bar{\rho}_{max}$ corresponds to $\varepsilon_t = \varepsilon_{t,min}$.

2.2 The stress level for compression steel is below the yield stress

The aforementioned equations utilized for developing the basic analysis of doubly reinforced beams with simplicity and accuracy are applicable solely if the compression steel yields when the beam attains its nominal strength. In numerous instances, including shallow sections, wide sections, those utilizing high yield strength steel, sections with minimal tensile reinforcement ratio, or sections featuring thicker concrete cover over the compression steel bars, the compression stress in compression bars will remain below the yield stress at the failure state. Considering the scenario where the compression reinforcement has not yielded at the point of flexural failure in the doubly reinforced beam, more generally applicable equations must be developed. The following steps can be used to determine whether compression steel yields at failure. Considering $\varepsilon'_s = \varepsilon_y$ as the limiting case, as shown in Figure 1(b),

$$\frac{c}{d'} = \frac{\varepsilon_u}{\varepsilon_u - \varepsilon_y} \text{ or } c = \frac{\varepsilon_u}{\varepsilon_u - \varepsilon_y} d'. \tag{10}$$

The minimum tensile reinforcement ratio ($\bar{\rho}_{cy}$) required to ensure compression steel yielding at failure is given by summing the forces in the horizontal direction (Figure 1(c)):

$$\bar{\rho}_{cy} = 0.85\beta_1 \frac{f'_c}{f_y}\frac{d'}{d}\frac{\varepsilon_u}{\varepsilon_u - \varepsilon_y} + \rho'. \tag{11}$$

If the tensile reinforcement ratio does not meet this limiting value, the neutral axis is elevated enough to prevent the stress in the compression steel at failure from surpassing the yield stress value. The balanced reinforcement ratio can easily be demonstrated using Figure 1(b) and (c) in this situation:

$$\bar{\rho}_b = \rho_b + \rho' \frac{f'_s}{f_y}, \tag{12}$$

where

$$f'_s = E_s \varepsilon'_s = E_s \left[\varepsilon_u - \frac{d'}{d}(\varepsilon_u + \varepsilon_y) \right] \le f_y. \tag{13}$$

To calculate ρ_{max}, $\varepsilon_t = \varepsilon_{t,min}$ is substituted for ε_y in equation (13), giving

$$f'_s = E_s \left[\varepsilon_u - \frac{d'}{d}(\varepsilon_u + \varepsilon_{t,min}) \right] \le f_y. \tag{14}$$

Thus, the maximum reinforcement ratio allowed for $\phi = 0.9$ is

$$\bar{\rho}_{max} = \rho_{max} + \rho' \frac{f'_s}{f_y}, \tag{15}$$

where f'_s is given by equation (14).

By comparing equations (12) and (15), with f'_s given by equations (13) and (14), respectively, it can be seen that equations (12) and (15) are referred to as generalized forms of equations (6) and (8). It is important to emphasize that equations (13) and (14) are only applicable to beams with exact strain values during the extreme tensile reinforcement of ε_y and $\varepsilon_t = \varepsilon_{t,min}$, only. If the ratio of tensile steel, ρ, is less than $\bar{\rho}_b$, as given by equation (12), and less than $\bar{\rho}_{cy}$, as given by equation (11), then the tensile reinforcement is at the yield stress at failure but the compression reinforcement is not, and compression steel's stress and flexural strength require new equations to be developed. The still-unknown neutral axis depth can be used to express the compression steel stress:

$$f'_s = \varepsilon_u E_s \frac{c - d'}{c}. \tag{16}$$

When the compression steel stress equals f'_s, the horizontal force equilibrium (Figure 1(c)) is considered, and it gives

$$A_s f_y = 0.85\beta_1 f'_c bc + A'_s \varepsilon_u A E_s \frac{c - d'}{c}. \quad (17)$$

The quadratic equation, with c as the sole unknown variable, can be solved efficiently. In order to determine the nominal flexural strength, we use f'_s from Eq. (4.41), where $a = \beta_1 c$ in the expression

$$M_n = 0.85 f'_c ab\left(d - \frac{a}{2}\right) + A'_s \ f'_s(d - d'). \quad (18)$$

The strength reduction factor ϕ is utilized to decrease this nominal capacity and achieve the design strength. The compression reinforcement becomes less likely to yield as the yield strength of the reinforcement increases. For example, the maximum strain in the concrete is 0.003, while the yield strain of Grade 100 reinforcement is 0.0034; therefore, Grade 100 reinforcement cannot yield in compression. To prevent compression bars from buckling outward under stress and causing spalling of the outer concrete, it is important to take precautions when using them in a flexural member. In ACI Code [3], reinforcement bars are required to be enclosed using closed stirrups or hoops, similar to the way compression bars in columns are enclosed by transverse ties. Transverse reinforcement is required along the entire length where compression reinforcement is necessary.

2.3 A summary of cases involving tension steel at yield stress

The first step is to check that the tensile steel ratio is lower than $\bar{\rho}_b$, given by equation (12), using compression stress from equation (13). After establishing that the tensile reinforcement reached its yield point, the tensile reinforcement ratio that indicates the yield of compression steel is determined using equation (11) and compared to the actual tensile reinforcement ratio. If it is higher than $\bar{\rho}_{cy}$, then $f'_s = f_y$, and M_n is determined using equation (5). If it is lower than $\bar{\rho}_{cy}$, then $f'_s < f_y$. In this case, c is determined by solving equation (17); f'_s is determined using equation (16) and M_n is determined using equation (18).

2.4 Tensile steel below the yield stress

To ensure beam yielding during failure, all doubly reinforced beams designed following the ACI Code [3] must be sub-reinforced by limiting the tensile reinforcement ratio. In Sections 2.1 and 2.2, two scenarios were discussed: (a) yielding occurs in both tensile steel and compression steel, and (b) yielding occurs in tensile steel while compression steel remains unyielded. Analyzing the capacity of the existing beams can result in two other combinations: (c) tension steel is not prone to yielding but compression steel is, and (d) neither type of steel is yielding. In reality, the last two cases are uncommon because creating such conditions would require a significant amount of tension reinforcement but the occurrence is possible. In these situations, the solution is obtained by simply extending the treatment of Section 2.2. An equation is created for horizontal equilibrium that uses the unknown neutral axis depth c to express both tension and compression steel stress. After solving the quadratic equation for c, steel stresses and nominal flexural strength can be calculated. The steps of analyzing doubly reinforced sections are illustrated in Figure 5.

Figure 5 presents a comprehensive flowchart that outlines the systematic analytical procedure for evaluating doubly reinforced concrete sections. The flowchart begins with the fundamental assumption that both tension and compression steel have yielded, and then proceeds through a series of decision points to verify this assumption against the calculated strain values. The process involves checking whether the actual tensile reinforcement ratio exceeds the balanced reinforcement ratio, determining if compression steel reaches yield stress, and calculating the appropriate nominal moment capacity based on these conditions. This iterative approach ensures accurate prediction of section behavior by accounting for different failure modes – whether tension-controlled, compression-controlled, or balanced failure occurs. The flowchart serves as a practical tool for engineers to systematically analyze doubly reinforced sections while avoiding common analytical pitfalls that can arise when assumptions about steel yielding prove incorrect.

Figure 6 illustrates the detailed reinforcement configurations for the three experimental beam specimens (B_1, B_2, and B_3) tested in this study. Each beam maintains identical overall dimensions of 1,750 mm span, 250 mm depth, and 100 mm width, with a consistent concrete cover of 8 mm and identical tension reinforcement consisting of two 22 mm-diameter bars. The key variable among the specimens is the compression reinforcement: B_1 incorporates two 10 mm-diameter bars, B_2 uses three 10 mm-diameter bars, and B_3 employs two 22 mm-diameter bars, resulting in compression-to-tension steel ratios of 0.2, 0.3, and 1.0, respectively. The schematic clearly shows the positioning of both longitudinal reinforcement and transverse

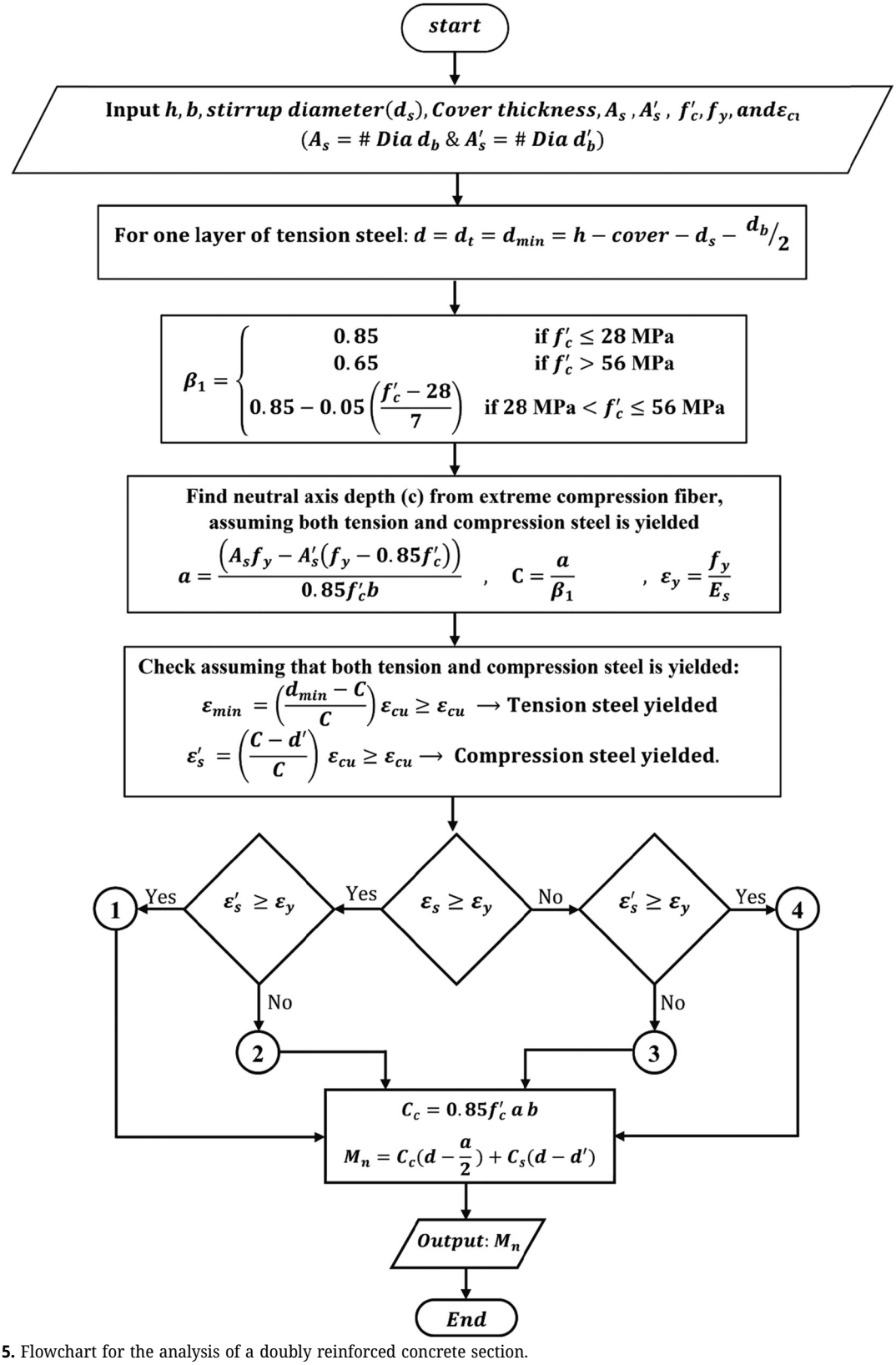

Figure 5. Flowchart for the analysis of a doubly reinforced concrete section.

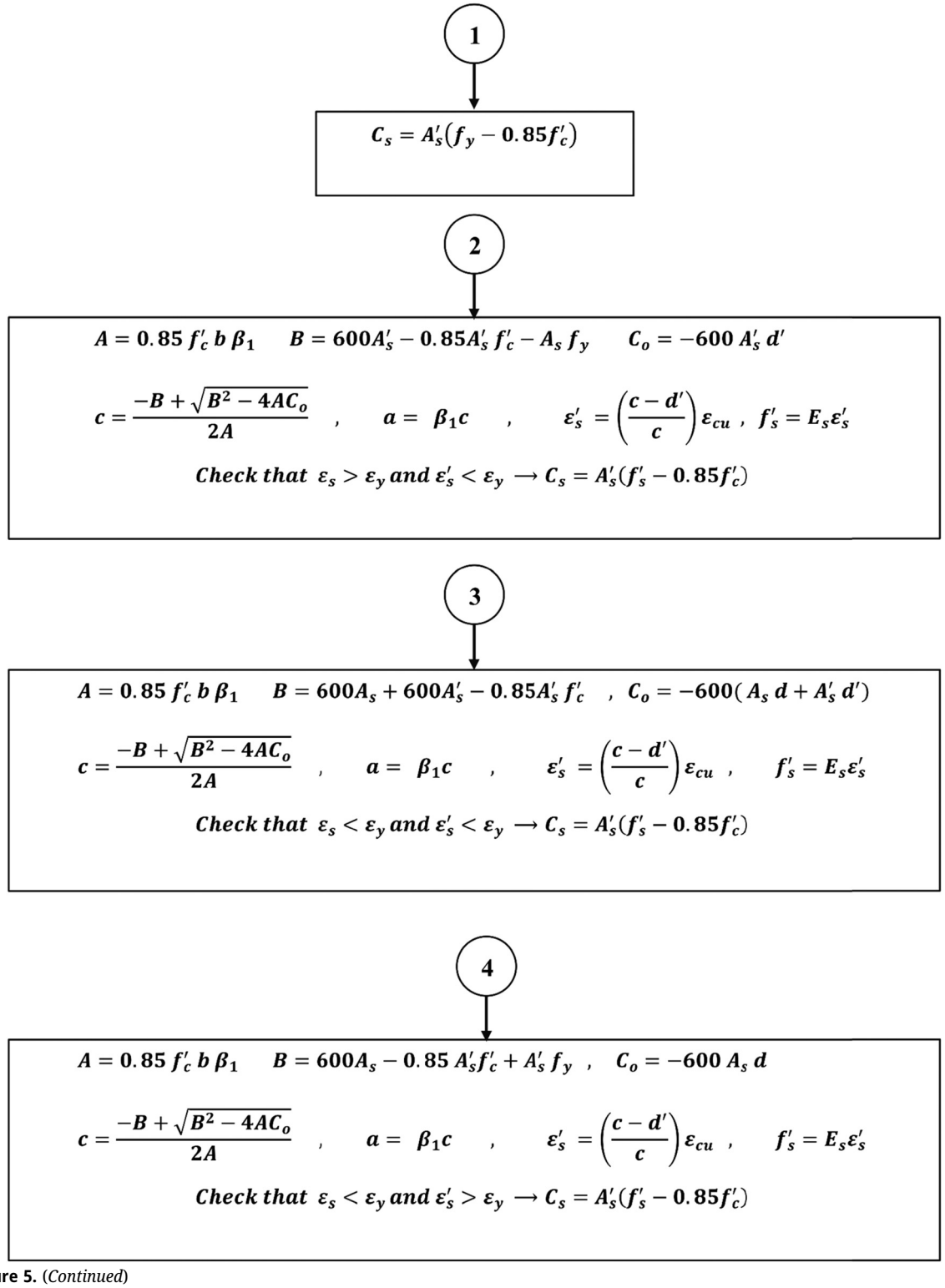

Figure 5. (*Continued*)

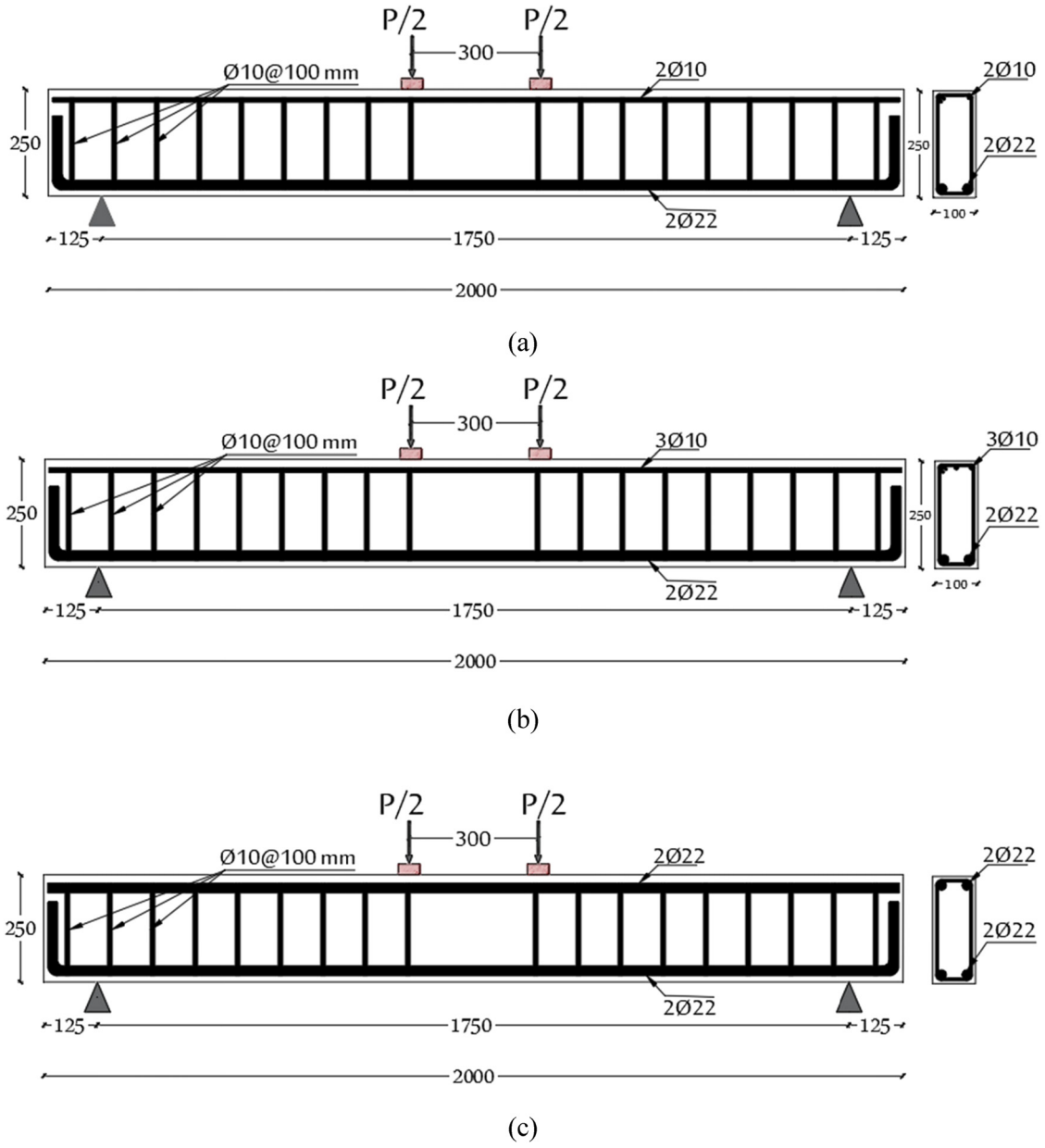

Figure 6. Schematic longitudinal and cross sections of the tested beams: (a) B_1, (b) B_2, and (c) B_3 (all dimensions in mm).

stirrups (10 mm diameter at 100 mm spacing), providing essential details for understanding the experimental setup. These configurations were specifically designed to investigate how varying amounts of compression reinforcement affect the structural behavior of shallow beams reinforced with high-strength Grade 500 steel, particularly their failure modes and ultimate load-carrying capacity.

3. Experimental program

3.1 Materials and concrete mix

Table 1 shows the concrete mix proportion for the specimen. According to ASTM C39 [27], the concrete mix's compressive strength is 25 MPa. The cement used in the

Cement	Dolomite	Sand	Water	Admixture
350 kg	1,292 kg	646 kg	175 L	5.4 kg

Table 1. Concrete mix proportion (m^3).

Beam ID	A_s	A_s'	A_s'/A_s	Details
B_1	2Ø22	2Ø10	0.2	Figure 6(a)
B_2	2Ø22	3Ø10	0.3	Figure 6(b)
B_3	2Ø22	2Ø22	1.0	Figure 6(c)

Table 2. Compression steel in the tested beams.

mixes was CEMI-52.5 N, in accordance with the European Standard EN [28]. This cement type was chosen for its high early strength development and consistent performance characteristics; type N (normal) designation provides a standard setting time suitable for laboratory casting procedures and complies with European Standard EN specifications, ensuring quality consistency. The fine aggregate utilized was natural siliceous sand, which meets the specifications outlined in EN196-1 [29]. The crushed dolomite stone was used as coarse aggregate in this investigation. This type was selected for its uniform mechanical properties and well-documented modulus of elasticity. Dolomite's known aggregate modulus (typically 2–3 times that of cement paste) provides a predictable contribution to concrete's elastic modulus calculations used in the proposed analytical method. A maximum size of 19 mm ensures adequate workability in the relatively narrow 100 mm beam width while maintaining representative aggregate-to-paste ratios. A high-range water-reducing Type F admixture was used. The water-to-cement ratio used in this study was 0.5. Three standard cylinders, each 300 mm in length and 150 mm in diameter, were manufactured and cured for 28 days under standard conditions until the test day. Deformed bars were utilized as reinforcement bars in this study, exhibiting a yield stress (f_y) of 500 MPa, which was tested according to ASTM A572 [30].

3.2 Specimen preparation

The dimensions and reinforcing details of the RC beams are illustrated in Table 2 and Figure 6. Three RC beams were fabricated with a cross section of 250 mm in depth and 100 mm in width, with a total length of 2,000 mm. The thickness of the concrete cover was 8 mm. The tension reinforcement bars (two with a 22 mm diameter) employed in the beams were identical, as shown in Table 2. The compression reinforcement bars were changed in all the beams as the major parameters in this study, where B_1 has two 10 mm-diameter, B_2 has three 10 mm-diameter, and B_3 has two 22 mm-diameter, as shown in Table 2. All the tested beams in this experimental study have the same constant parameters, including the loading, shear force, and bending moment diagrams, as shown in Figure 7.

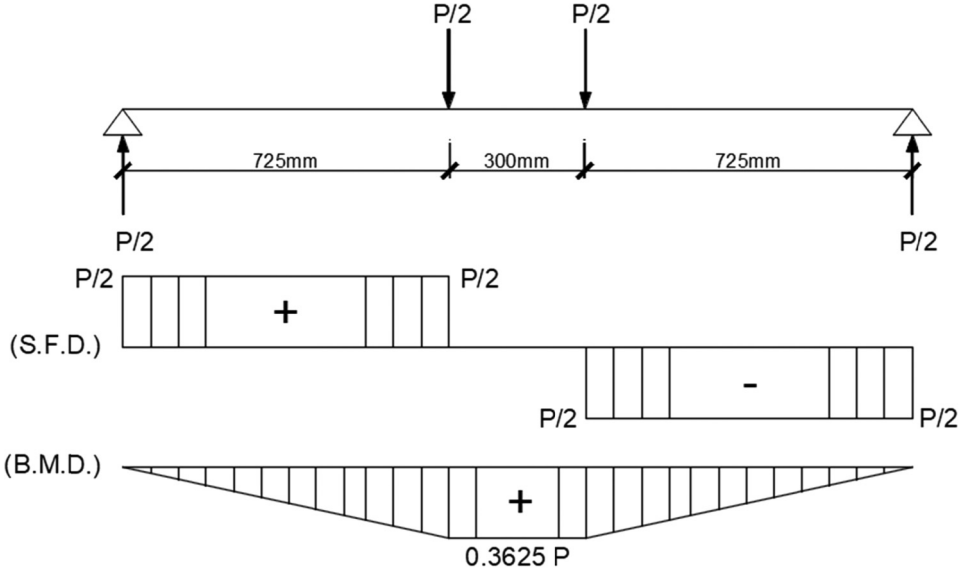

Figure 7. Loading, shear force, and bending moment diagrams of the tested beams.

Figure 8. Concrete pouring of the beam specimens and cylinders.

The beams were cast following the guidelines outlined in ASTM C31 [31]. A portable vibrator was utilized to eliminate trapped air and achieve optimal compaction. Following casting, a trowel was employed to ensure that the surface of the beam was level. Subsequently, the beams' surfaces were enveloped in moist burlap. The formwork was taken off after 24 h. The beams were cured for 28 days in accordance with ACI-308R-01-R08 [32]. Figure 8 shows the beam specimens and cylinders during concrete pouring. Reinforcement cages of the tested beams are shown in Figure 9.

3.3 Instrumentation

To assess the variance of strain as a function of the loading, five strain gauges were installed on every beam. One strain gauge, ST1 (Tokyo, gauge length 60 mm), was installed directly at the top of the concrete layer. Two strain gauges, designated as ST2 and ST3 (Kyowa, with a gauge length of 10 mm), were positioned at the upper reinforcement bar within the compression zone. Two strain gauges, ST4 and ST5 (Kyowa, gauge length 10 mm), were positioned at the bottom reinforcement bar. All gauge locations correspond to points of maximum expected strain in their respective materials. The measurement points align with the theoretical strain distribution assumptions used in the proposed analytical method. Placement enables direct comparison between experimental strain profiles and analytical predictions. For instance, ST1 is positioned at the extreme compression fiber to capture the maximum compressive strain in concrete. The longer gauge length (60 mm) averages strain over a representative concrete volume, reducing localized effects from aggregate distribution or surface irregularities. It is critical for validating the proposed analytical model's assumption that failure occurs at $\varepsilon_o \approx 0.0015$ rather than the conventional 0.003. In addition, ST2 and ST3 were positioned to directly measure whether compression reinforcement reaches yield strain (0.0025), which is fundamental to the analytical approach selection in the flowchart (Figure 5); ST2 and ST3 were strategically located in the maximum moment region where tensile strains are highest. The deflections at the midspan of the evaluated

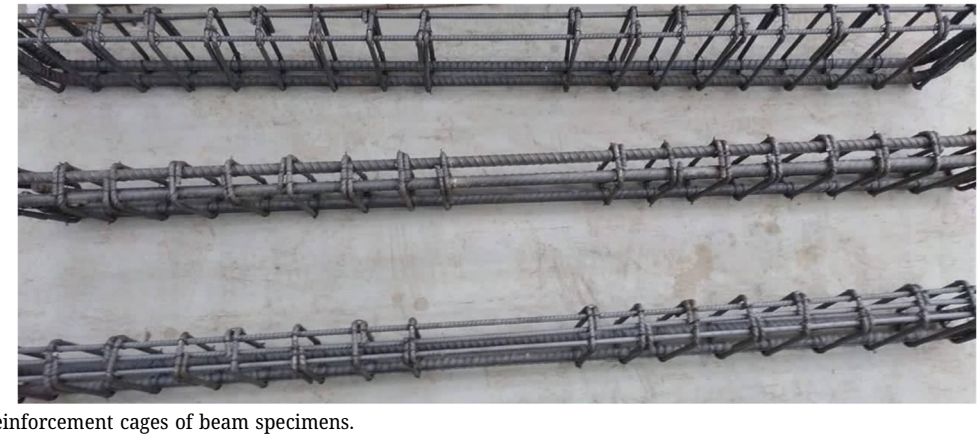

Figure 9. Reinforcement cages of beam specimens.

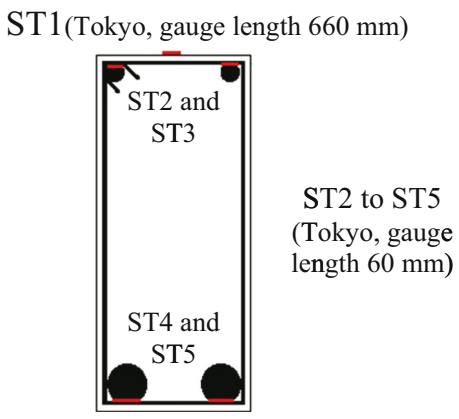

Figure 10. Positions of strain gauges.

beams were measured using linear variable displacement transducers (LVDT). A data logger was employed to record the data from the LVDT and electrical strain gauges. Figure 10 shows the strain gauges used.

3.4 Test procedure

The four-point flexural test was adopted for testing all beams with the central section subjected to pure bending, i.e., without shear effect. A Shimadzu Universal Testing Machine (UTM) with a 500 kN capacity was employed to load the beams monotonically. The crack propagation, mode of failure, and failure load for each beam were recorded. Figure 11 shows the test setup and locations of LVDTs. The clear span of the beam measures 1,750 mm, with the two loading points positioned 300 mm, symmetrically located around the midspan of the beam. The shear span measured was 725 mm for the tested beams. For each stage of loading, strains are measured at the maximum compression fiber of concrete, compression steel, and tension steel.

4. Results and discussion

4.1 Mode of failure

All beams experienced failure as a result of concrete crushing in the maximum moment region, as illustrated in Figure 12. In addition, all beams experienced compression-controlled failure, even B_3, which has $A_s = A'_s$. The failure mode for all beams is depicted as a classic compression-controlled failure, as defined by ACI 318. The primary visual evidence for this classification is as follows: (i) the major feature was concrete crushing and spalling of concrete in the maximum moment area, especially on the top compression face of the beam. It is clearly shown in Figure 12, which reflects broken concrete pieces and exposed reinforcement after failure; and (ii) this failure mode occurred without significant yield of tensile reinforcement. There was no noticeable widening of flexural cracks or adequate deflection warning before the sudden crushing of concrete. This indicates that compressed stress in concrete reached its final capacity before tensile steel reached its yield stress. The compression-controlled failure refers to a failure mode in reinforced concrete members that occurs when the concrete reaches its ultimate compressive strain (typically 0.003) before the tensile

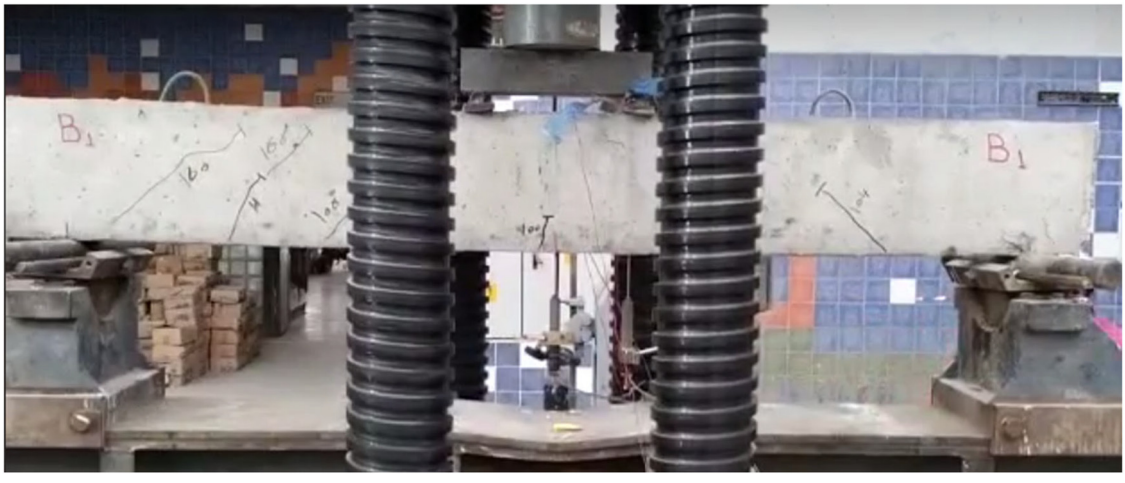

Figure 11. Test setup.

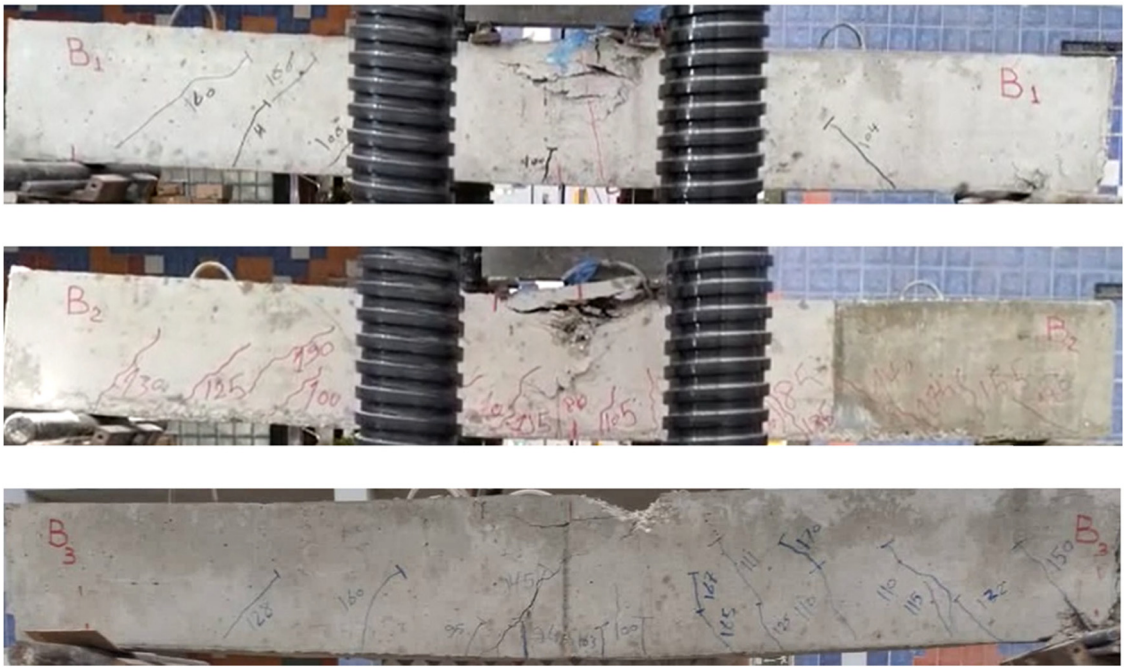

Figure 12. Compression-controlled failure of all the tested beams.

reinforcement yields. This type of failure is characterized by crushing of concrete in the compression zone and is typically sudden and brittle in nature. According to most design codes (ACI318, SBC304), compression-controlled sections have a net tensile strain in the extreme tensile reinforcement at a nominal strength of less than the yield strain when the concrete reaches its assumed ultimate compressive strain. This failure mode is associated with over-reinforced sections and is generally avoided in design to ensure ductile behavior. Figure 12 illustrates the final propagation of cracks upon failure for all test beams. The crack patterns are generally similar. Initially, vertical cracks appeared at the midspan within the flexural region in all beams, followed by additional cracks that extended toward the loading points as the load increased. Furthermore, hairline cracks began at midspan and gradually extended toward the neutral axis of the beam during the initial loading phase until the concrete failed on the compression side. Subsequently, inclined cracks, characterized as flexural-shear cracks, emerged within the bending shear zone. Figure 12 clearly illustrates that the extent of damage to the compression zone of the B_1 beam is significantly greater than that observed in the B_2 and B_3 beams, which indicates that as the compressive steel bars increased, the concrete damage diminished. The B_3 beam exhibited greater deformations than all beams but experienced a brittle failure, predominantly on the compression side. After the beam reached compression failure, some tensile cracks appeared under loads exceeding the compression failure load. However, this additional load is disregarded since the beam had already failed in compression – a sudden failure mode that occurs without any prior warning.

4.2 Load–deflection and load–strain curves

Figure 13 illustrates the load–deflection curves for all beams. The load–deflection response of all beams was approximately consistent. The load increase for the beams demonstrates nearly bilinear characteristics. Following the attainment of its maximum load, there is a notable abrupt interruption of the curves, as illustrated in Figure 13. This interruption can be attributed to concrete crushing in the compression region, resulting in its ultimate failure. Therefore, the test was terminated at this load level. Figure 13 illustrates that the B_1 and B_2 beams rapidly lose their capacity to support load shortly after attaining the peak load. Conversely, in the case of the B_3 beam, there is a slight reduction in load immediately after reaching the peak load; however, the B_3 beam continues to support the remaining load, as evidenced by the minor plateau that formed. Figure 13 and Table 3 demonstrate

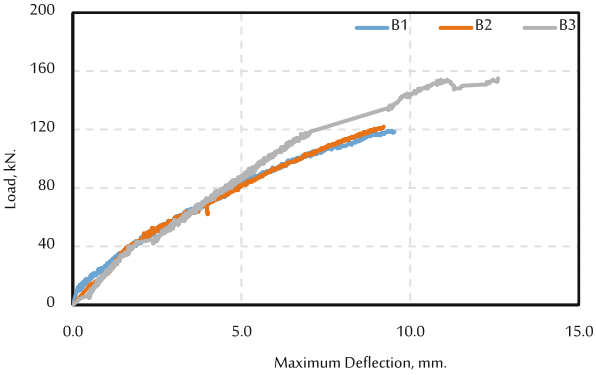

Figure 13. The relationship between load and maximum deflection for the tested beams.

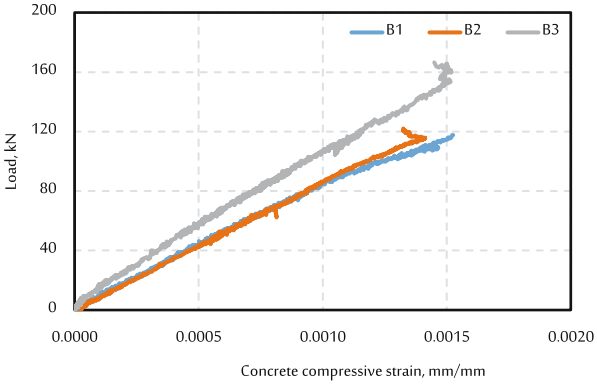

Figure 14. The relationship between load and maximum concrete compressive strain for the tested beams.

that the increase of steel bars in the compressive region significantly enhanced the load-carrying capacity of the beams. The B_1 beam exhibited a failure at a peak load of 118.4 kN, whereas the B_2 beam, which included 3Ø10, failed at a peak load of 122 kN, and the B_3 beam had a peak load of 166 kN. The use of 3Ø10 in the B_2 beam showed a slight increase in the load-carrying capacity by 3% compared to the B_1 beam (with 2Ø10). In addition, the B_3 beam (with 2Ø22) showed the highest load-carrying capacity compared to all beams, with an increased ratio of 40.2 and 36.1% compared to the B_1 and B_2 beams, respectively. The B_3 beam demonstrated the capacity for further deflection beyond the peak load, a characteristic that was absent in the B_1 and B_2 beams. The B_3 beam demonstrated a more significant deflection of approximately 3 mm following the attainment of the peak load and upon the onset of concrete crushing at the extreme top fiber. The test results are summarized in Table 3, including the load, maximum deflection, strain at maximum compressive fiber, strain at tension steel, and strain at compression steel at failure. The nominal moment strengths for all beams were calculated, as illustrated in Figure 7. The B1 beam had a nominal moment strength of 42.92 kN m, whereas 44.23 kN m for the B_2 beam with 3Ø10, and 60.18 kN m for the B3 beam with 2Ø22. Using 3Ø10 in the B_2 beam resulted in a 3% increase in the nominal moment strength compared to the B_1 beam (2Ø10). The B_3 beam (with 2Ø22) had the highest nominal moment strength among all beams, with higher ratios of 40.2 and 36.1% compared to the B1 and B2 beams, respectively.

Figure 14 shows the relation between load and compressive strain in concrete till failure occurs. The curves increased almost linearly across all beams. No significant difference was observed between the B_1 and B_2 beams, while the B_3 beam experienced a significant increase compared to the other beams. The most important result is that compression strain in concrete at failure is around 0.0015 and not 0.003 as in all provisions and codes. Figures 15 and 16

Point of comparison	B_1 beam			B_2 beam			B_3 beam		
	Experimental	Analytical	%	Experimental	Analytical	%	Experimental	Analytical	%
Failure load (kN)	118.4	105.9	+11.8%	122.0	111.1	+9.8%	166.0	150.2	+10.5%
Nominal moment strength* (kN m)	42.92	38.39	+11.8%	44.23	40.27	+9.8%	60.18	54.45	+10.5%
Concrete compressive strain at failure	0.001526	0.001507	+1.3%	0.001413	0.001507	−6.2%	0.001518	0.001507	+0.7%
Strain in tension steel at failure	0.001376	0.001365	+0.8%	0.001460	0.001446	+1.0%	0.001765	0.001729	+2.1%
Strain in compressive steel at failure	0.001344	0.001330	+1.1%	0.001211	0.001194	+1.4%	0.000979	0.001054	−7.1%

*Bending moment due to the weight of the beam is neglected.

Table 3. Comparison of experimental and proposed method results.

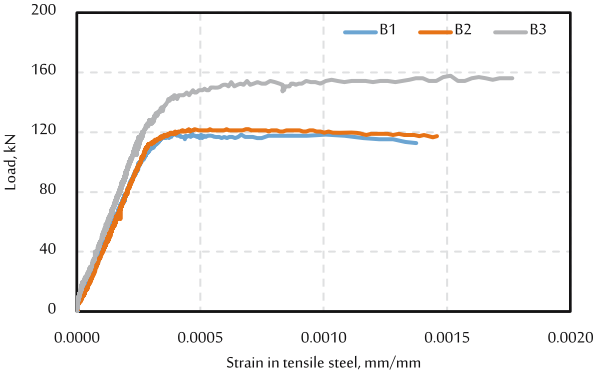

Figure 15. The relation between load and strain in tensile steel for the tested beams.

illustrate the load–strain curve for strain in tension reinforcement and strain in compressive steel, respectively, for the tested beams. The strains recorded by the strain gauges placed on both bars of the bottom and top (tension and compression bars) were approximately identical for each specified location, which was common for all strain gauges. The strain at every point was determined by averaging the values obtained from the two strain gauges associated with that specific point. For instance, the strain measured at the compressive reinforcement bars of the beam was calculated as the average of ST2 and ST3, while the average of ST4 and ST5 was for the tension reinforcement bars, as illustrated in Figure 10. The curves initially exhibit a linear progression, with B_1 and B_2 beams displaying identical trends with minor discrepancies. The B_3 beam exhibits a significant disparity at the same deflection level. The curves for B_1 and B_2 beams exhibit a linear growth until they attain a load of roughly 110 kN. The load thereafter exhibits a minor increase before stabilizing, accompanied by a notable increase in strains. The B_3 beam curve persists in a linear ascent until reaching a load of roughly 130 kN. The load thereafter exhibits a minor increase before stabilizing, accompanied by a substantial increase in strain. The curves indicate that the reinforcement bars in the tension zone have not yielded, as the strain values have not attained the yield strain threshold (0.0025), as illustrated in Figure 15. Regarding the strain in compressive steel, the same trends were noticed in tension steel, where the load–strain responses show a linear increase in the first part of the curves, and then the curves turn into a non-linear response, as illustrated in Figure 16. The curves demonstrate that the compressive reinforcement bars have not yielded, as the strain values have not reached the yield strain threshold (0.0025). Nonetheless, the results indicated that the strain values in the compression steel were lower than those in the tensile steel, as illustrated in Figures 15 and 16.

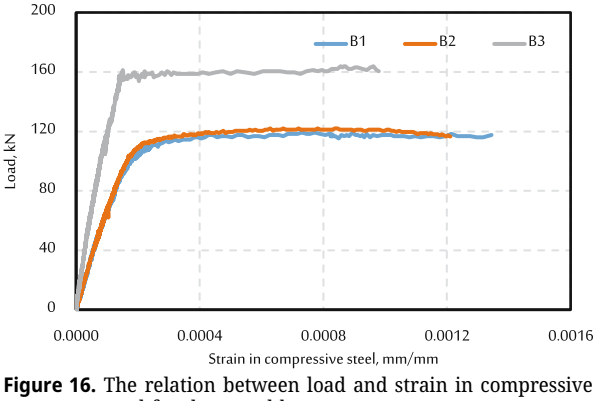

Figure 16. The relation between load and strain in compressive steel for the tested beams.

The load–deflection behavior observed in Figure 13 reveals fundamental differences in how these beams redistribute internal forces as they approach failure. The bilinear characteristics observed in all three beams reflect a two-stage loading process inherent to reinforced concrete behavior. (i) Initial linear stage: both concrete and steel behave elastically, with loads shared proportionally according to their respective elastic moduli. The slope of this portion corresponds to the composite section's flexural rigidity (EI); (ii) second stage (reduced stiffness): as loads increase, concrete begins developing microcracks in the tension zone, progressively reducing the section's effective moment of inertia. This creates the characteristic stiffness reduction visible in the curves. In addition, the plateau exhibited by B_3 (A_s'/A_s = 1.0) versus the abrupt failure of B_1 and B_2 stems from fundamentally different internal force redistribution mechanisms, where B_1 and B_2 beams (lower compression steel ratios) have a limited compression reinforcement (A_s'/A_s = 0.2 and 0.3) and cannot effectively redistribute compressive forces when concrete approaches its limiting strain. Upon reaching $\varepsilon_o \approx 0.0015$, the concrete crushes suddenly with insufficient steel to maintain equilibrium. This results in brittle, compression-controlled failure with immediate load-carrying capacity loss, while the B_3 beam (equal reinforcement ratio) has a substantial compression steel (A_s'/A_s = 1.0) that creates a more balanced internal force system. When concrete reaches limiting strain, the compression reinforcement can temporarily maintain some load-carrying capacity. This allows continued deformation under reduced but sustained loading, creating the observed plateau. The beam essentially transitions to a "steel-dominated" compression zone after concrete crushing. The experimental data support this explanation that B_3 demonstrated continued deflection capacity (approximately 3 mm beyond the peak load) because its compression steel, while not yielding (strain < 0.0025), provided sufficient reserve capacity to prevent

immediate collapse. In contrast, B_1 and B_2 lacked this reserve, leading to sudden failure once the concrete compressive capacity was exhausted. This behavior confirms that while increasing compression steel improves post-peak ductility, it cannot prevent the fundamental problem of compression-controlled failure in shallow beams with high-strength steel, as the reinforcement utilization remains suboptimal (strains well below yield in both tension and compression steel).

4.3 Analysis of the results

Analysis of the tested beams using the conventional method of such a doubly reinforced section, as shown in Figure 5, always fails. For example, starting with the assumption that both tension and compression steel yielded in the first trial does not match with the strains at the end of this trial, so in the second trial, we started with the strains at the end of the first trial, but, at the end, the strain in either tension steel or compression steel or both yielded. Therefore, we needed a third trial and so on, and the analysis did not converge, even after several trials. This could be due to many reasons, such as:

- Strain at failure is almost equal to around 0.0015, not 0.003, as proposed by the code.
- High-grade steel with a yielding stress = 500 MPa, accompanied by a shallow depth causes the impossibility of the compression steel to reach yielding.
- Shallow depths also limit strain to reach the strain at which the section will be considered tension-controlled (0.003 + 0.0025 = 0.0055). The strain values for tension reinforcement bars may be less than the yield strain, so compression failure occurs in all three beams, even B_3, which has $A_s = A_s'$.

Therefore, the conventional calculations could not be used in these shallow beams reinforced by high-grade steel with a yield stress equal to 500 MPa. Building codes, including those from the ACI code [3], generally specify a 0.003 as the maximum compressive strain of concrete subjected to flexural load. This value represents a simplified and conservative estimate that considers the intricate stress–strain behavior of concrete to ensure a margin of safety. Although 0.003 is commonly applied in designs, the actual strains at failure were different. The actual strain at concrete failure is influenced by factors such as the concrete mix, reinforcement grade, and reinforcement confinement. Consequently, it is imperative to develop an analytical approach that ensures high precision, particularly for the design of doubly reinforced shallow beams utilizing grade 500 steel.

5. Proposed analysis of sections

From the above discussion of the results, it is obvious that the conventional calculations of such shallow beams are not suitable for determining their flexural capacity, especially if they are reinforced by high-grade steel. In this research, the authors developed a proposal to analyze these sections.

5.1 Initial, tangent, and secant moduli of elasticity

First, we determined the value of the modulus of elasticity of concrete, E_c. Figure 17 illustrates three methods for defining the modulus of elasticity. The tangent modulus of elasticity (E_T) at a specified stress is determined by the slope of the tangent line at a particular point on the stress–strain curve, for instance, point A. The slope of the curve at the origin point is referred to as the initial tangent modulus. Meanwhile, the secant modulus of elasticity for a specific stress is calculated as the slope of a line drawn from the origin point to the corresponding point on the stress–strain curve (e.g., point B in Figure 17). The secant modulus is often determined using the stress point associated with $0.4f_c'$ to represent service-load stresses. The slopes of these lines are measured in psi (MPa) per unit strain, making the modulus of elasticity's unit psi (MPa) since strain is dimensionless.

The initial tangent modulus of elasticity, the initial slope of stress–strain curves, increases with increased compressive strength. The modulus of elasticity of concrete (E_c) is affected by the modulus of both the aggregates and the cement paste. Raising the water-to-cement ratio elevates paste porosity, hence diminishing its strength and modulus. Design practices address this by relating E_c to f_c'. The aggregate's modulus is equally crucial. Normal-weight aggregates have moduli ranging from 1.5 to 5 times the modulus of the cement paste, indicating that their proportion in the mix significantly impacts E_c. Conversely, lightweight aggregates have moduli similar to the paste, so their proportion minimally affects E_c in lightweight concrete. According to ACI Code [3], the modulus of elasticity for concrete with densities ranging from 1,440 and 2,560 kg/m^3 is calculated as

$$E_c = w_c^{1.5} 0.043 \sqrt{f_c'} \quad \text{(in MPa)}, \tag{19}$$

where w_c is the concrete density in kg/m^3.

This formula, derived from short-term tests on concrete within the specified density range, represents the

secant modulus at approximately $0.50f'_c$ [33]. The initial tangent modulus is about 10% higher. Since equation (19) does not account for aggregate type, data variability is significant. It tends to overestimate E_c in regions with low-modulus aggregates. Therefore, when design considerations involve deflections or vibration characteristics, it is advisable to measure E_c for the specific concrete used.

For normal-weight concrete, the ACI Code provides [3]

$$E_c = 4{,}700\sqrt{f'_c} \quad \text{(in MPa)}. \tag{20}$$

Additionally, ACI Committee 363 [34] suggests the following for high-strength concretes:

$$E_c = 3{,}300\sqrt{f'_c} + 7{,}000 \quad \text{(in MPa)}. \tag{21}$$

Equations (19)–(21) offer practical means to estimate concrete's modulus of elasticity based on its compressive strength and density.

5.2 Stress–strain relationship for normal-weight concrete under compressive loads

Figure 18 presents standard stress–strain responses for concretes with varying strength classifications, derived from approximately 15-min tests on specimens analogous to a beam's compression zone. These curves exhibit an ascending branch that peaks at maximum stress, corresponding to strains ranging from 0.0015 to 0.003, subsequently followed by a descending segment. The shape of the ascending branch is attributed to the gradual development of microcracks within the concrete's structure. Notably, five key properties can be identified from these curves, which are instrumental in formulating mathematical models for concrete's compressive stress–strain behavior [35].

The ascending segment of the concrete stress–strain curve is often approximated by a parabola peaking at the maximum stress [35,36]. This parabolic approximation is commonly employed for computational purposes. As concrete strength increases, the ascending portion of the curve tends to straighten [37]. As concrete compressive strength increases, the strain at maximum stress (ε_o) also increases.

5.3 Equations for compressive stress–strain diagrams

The modified Hognestad stress–strain curve [9] is a widely accepted model for representing the behavior of concrete under compression, particularly for concretes with strengths up to approximately 42 MPa. This model provides a parabolic approximation of the ascending portion of the stress–strain curve, as depicted in Figure 19,

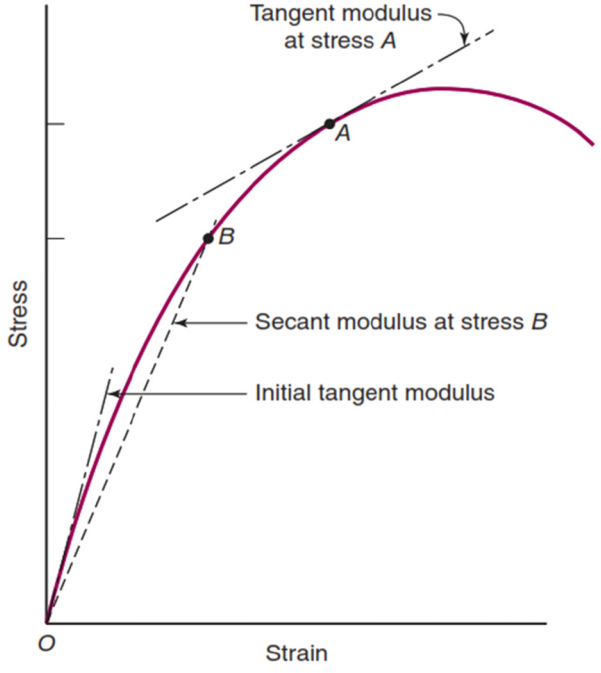

Figure 17. Initial, tangent, and secant moduli of elasticity of concrete [9].

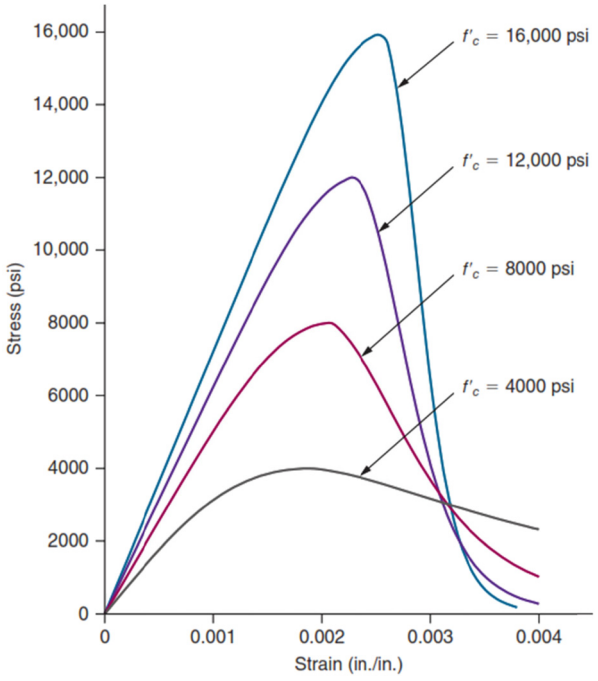

Figure 18. Typical concrete stress–strain curves in compression [9].

culminating at the peak stress, and is commonly used for computational analyses.

5.4 Proposed analytical model for shallow beams

The experimental results indicate that shallow beams fail once the concrete compressive strain reaches ε_0, without exhibiting the descending segment of the stress–strain curve. In the proposed analysis method, the ascending parabolic portion of the stress–strain curve is utilized without modifications, as depicted in Figure 20. This approach differs from conventional methods that often adjust this portion of the curve for simplification. By retaining the original parabolic shape, the analysis aims to more accurately represent the material's behavior under load.

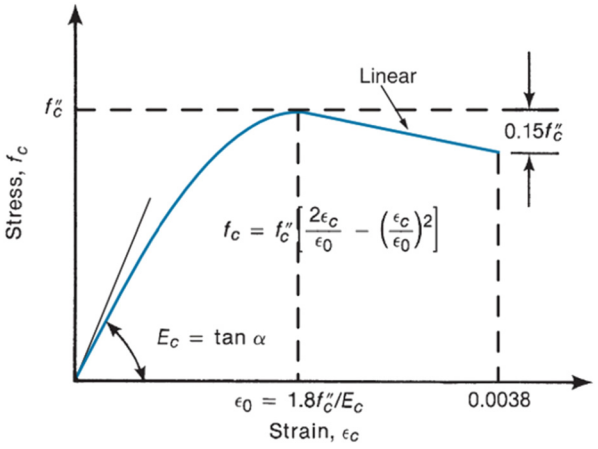

Figure 19. Analytical approximation to the compressive stress–strain curve for concrete [9].

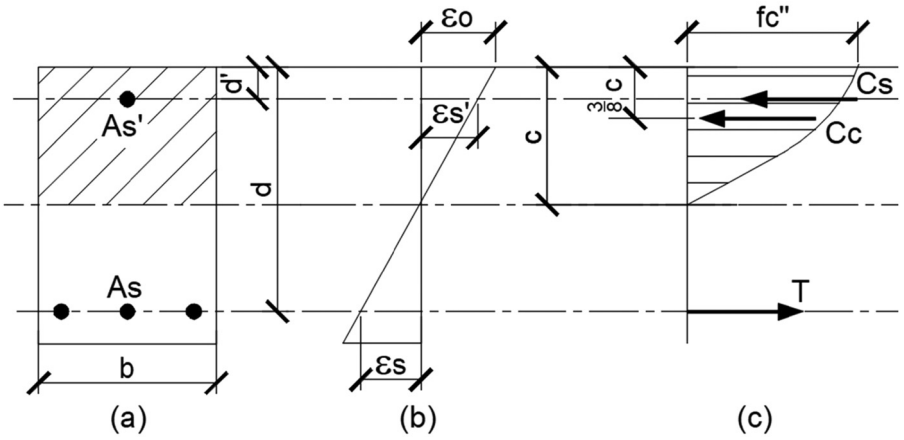

Figure 20. Proposed analytical model for shallow beams. (a) Cross-section, (b) Strain distribution, and (c) Stress and forces.

5.4.1 Steps of the proposed method

In this analysis, E_c is determined using equation (19). The measured concrete density (w_c) averaged 2,500 kg/m^3 in laboratory tests, leading to an E_c value of 26,875 MPa.

As shown in Figure 19, f_c'' is calculated as

$$f_c'' = 0.90 \quad f_c', \tag{22}$$

$$\varepsilon_o = \frac{1.8 \quad f_c''}{E_c} = \frac{1.62 \quad f_c'}{E_c}. \tag{23}$$

In this investigation, f_c'' = 22.5 MPa and ε_o = 0.001507 ≈ 0.0015.

In the proposed analysis method, the equations are consistent with those presented in Figure 5, with the following key differences:

1. Compressive force in concrete (C_c): Determined using equation (24), which accounts for the parabolic stress distribution:

$$C_c = \frac{2}{3} \times 0.9 f_c' \times c \times b = 0.6 f_c' \times c \times b. \tag{24}$$

2. The location where the concrete compressive force is applied is as follows: Unlike conventional beams, where the compressive force is assumed to act at the centroid of a rectangular stress block (typically at $a/2$), in this method, the force is considered to act at the centroid of the parabolic stress distribution, located at $3/8c$.
3. Compressive force in steel reinforcement (C_s): Calculated using equation (25), this method subtracts $0.9 f_c'$ instead of the traditional $0.85 f_c'$, reflecting a more precise assessment of the steel's contribution to the overall compressive force:

$$C_s = A_s' \times (f_s' - 0.9 f_c'). \tag{25}$$

In equation (25), if the compression steel reaches its yield strain, the yield strength (f_y) is used in place of stress in the compression reinforcement (f_s'). This substitution reflects that the compression steel has yielded, and its stress equals its yield strength. Conversely, if the compression steel has not reached its yield strain, f_s' is calculated based on the actual strain in the compression reinforcement. This approach ensures an accurate representation of the compression steel's contribution to the overall structural behavior.

These adjustments aim to provide a more accurate representation of the actual stress distribution within the concrete and the contribution of the steel reinforcement.

5.5 Comparison of experimental and proposed method results

The primary outcomes of the proposed analytical method, alongside the corresponding experimental findings, are summarized in Table 3. The analysis of the experimental results compared to the analytical results proposed by the authors indicates the following:

1. The strains are very similar, exhibiting an error of approximately 7%.
2. The difference in the ultimate load or the maximum bending moment the beam can withstand is within approximately 11%, with the experimental results being higher than the analytical calculations.

The error percentages were calculated using the standard relative error formula:

$$\text{Error}(\%) = \frac{\text{Experimental Value} - \text{Analytical Value}}{\text{Experimental Value}} \times 100. \quad (26)$$

They show remarkable consistency (8.9–10.6% range), indicating the proposed method's reliability across different compression steel ratios. The results are generally consistent, except for B_3 compression steel strain (7.7% error). This outlier is likely to reflect the higher sensitivity in compression steel behavior at $A_s'/A_s = 1.0$ ratio, potential local effects in the heavily reinforced compression zone, and small absolute strain values amplifying relative error calculations. The error distribution suggests that the proposed method provides reliable predictions across the tested range, with slightly higher uncertainty in compression steel strain for heavily reinforced sections. This level of accuracy compares favorably with other analytical methods for reinforced concrete (typically 10–15% variation).

Accordingly, the proposed calculations can predict the strength of these shallow beams reinforced with high-strength steel, yielding results on the safe side compared to traditional calculations, which fail to provide an accurate analysis for such beams.

6. Conclusions

Sometimes, architectural considerations require the use of hidden beams instead of projected beams. As a result, the beam depth is limited by the depth of the concrete slab, making it necessary to use compression reinforcement, which may be equal to the tensile reinforcement, to compensate for the reduced concrete section depth. If these shallow beams are reinforced with high-yield-strength steel (500 MPa), traditional calculations are not suitable for predicting the beam section's resistance to bending moments. This is because the beam fails before the maximum strain in the concrete on the compression side reaches 0.003, as specified in most design codes. Experimental tests were conducted on three beams to investigate their behavior, with the compression reinforcement ratio to tensile reinforcement set at 0.2, 0.3, and 1.0. The strains in the concrete, tensile reinforcement, and compression reinforcement were measured, along with the failure load of these beams. Instead of the conventional method, a proposed method has been developed to analyze these sections. The proposed analytical calculations accurately predict the strength of shallow beams reinforced with high-strength steel, as evidenced by the close agreement between experimental and analytical strain results and the slight (approximately 11%) conservatism in ultimate load predictions, ensuring a safer assessment compared to traditional methods. From the above, it is evident that using high-strength steel on the compression side along with steel on the tension side in shallow beams, even if their ratio is 1, will not solve the issue of compression-controlled failure. Such failure will still occur, making this solution uneconomical. This is because the strain in both the tension and compression reinforcement will likely not reach the yield strain, meaning we will not fully utilize the strength of the used steel. Additionally, a reduction factor of $\phi = 0.65$ will be applied instead of $\phi = 0.90$, which is used in tension-controlled failure. This means that we will only utilize 72% of the strength that could have been used, making this solution highly uneconomical. Therefore, it is not recommended unless absolutely necessary.

7. Recommendations

The authors recommended expanding this study through the following:

- Phase 1: Investigating the parametric studies, such as the effects of beam depth, steel grade, and reinforcement ratio, to develop specific correction factors and analytical models.
- Phase 2: Studying the influence of material properties, such as concrete strength and aggregate type, on reinforcement efficiency.
- Phase 3: Focusing on design optimization through cost analysis and the exploration of alternative solutions like high-strength concrete.
- Phase 4: Developing simplified design guidelines and support code modifications for the practical application of the findings.

Acknowledgments

The authors gratefully acknowledge the funding of the Deanship of Graduate Studies and Scientific Research, Jazan University, Saudi Arabia, through Project number JU-202503163-DGSSR-RP-2025.

Author contributions

All authors contributed to the work equally.

Conflict of interest statement

Authors state no conflict of interest.

Data availability statement

The datasets generated during the current study are available from the corresponding author on reasonable request.

References

[1] Shariat, M., Shariati, M., Madadi, A., Wakil, K., Computational Lagrangian Multiplier Method by using for optimization and sensitivity analysis of rectangular reinforced concrete beams, Steel Compos. Struct., 2018, 29: 243–256

[2] Reynolds, C.E., Steedman, J.C., Threlfall, A.J., Reinforced concrete designer's handbook, CRC Press, USA, 2007

[3] ACI 318M-14, Building code requirements for structural concrete (ACI 318M-14): an ACI Standard: Commentary on building code requirements for structural concrete (ACI 318M-14), American Concrete Institute, USA, 2015

[4] Saini, B., Sehgal, V.K., Gambhir, M.L., Genetically optimized artificial neural network based optimum design of singly and doubly reinforced concrete beams, Asian J. Civ. Eng., 2006, 7(6): 603–619

[5] Jabbar, A.M., Hasan, Q.A., Abdul-Husain, Z.A., A theoretical study to predict the flexural strength of singly and doubly reinforced ultra-high performance concrete beams, J. Eng. Sci. Technol. Rev., 2022, 15: 91–101

[6] Bhalchandra, S.A., Adsul, P.K., Cost optimization of doubly reinforced rectangular beam section, Int. J. Mod. Eng. Res., 2012, 2: 3939–3942

[7] Manjunath, H.R., Kavya, K.R., Rao, K., Prakash, M.R., Prabhakara, R., Analysis of flexural behaviour of singly and doubly reinforced high strength concrete beams using ANSYS, In Proceedings of International Conference on Advances in Architecture and Civil Engineering (AARCV 2012), 2012, p. 179

[8] Galeb, A.C., Optimum design of doubly reinforced concrete beams using simulated annealing, Int. J. Civ. Eng. Technol. (IJCIET), 2018, 9: 61–70

[9] Wight, J.K., Reinforced concrete: Mechanics and design, 8th ed., Prentice Hall, Upper Saddle River, NJ, 2022

[10] Tahwia, A.M., Noshi, A., Abdellatief, M., Matthana, M.H., Experimental investigation of rubberized concrete slab-on-grade containing tire-recycled steel fibers, Innovative Infrastruct. Solut., 2024, 9: 46

[11] Handousa, A.M., Abdellatief, M., Salem, F.A., Mahmoud, N., Ghannam, M., Experimental and analytical study on axial behaviour of square corrugated concrete filled single and double skin tube stub columns, Sci. Rep., 2025, 15: 2167

[12] Eurocode 2: Design of concrete structures–part 1, Eurocode 2: Design of concrete structures-part 1–1: General rules and rules for buildings, Eur. Comm. Standard. Bruss., 2004, 668: 668

[13] CSA, Design of concrete structures, A23.3-04, Canadian Standards Association, Canada, 2004

[14] SBC, The Saudi Building Code for concrete structures and commentary, The Saudi Building Code National Committee (SBCNC), Riyadh, KSA, 2018

[15] ECP (Egyptian Code of Practice), The Egyptian Code for the Design and Construction of Concrete Structures, Housing and Building National Research Center, Giza, Egypt, 2020

[16] Hassoun, M.N., Al-Manaseer, A., Structural concrete: theory and design, John Wiley & Sons, USA, 2020

[17] Darwin, D., Dolan, C.W., Nilson, A.H., Design of concrete structures, McGraw-Hill Education, New York, NY, USA, 2016

[18] Ghoneim, M., EI-Mihilmy, M., Design of reinforced concrete structures, 2nd ed., Cairo University, Giza, Egypt, 2008

[19] Bhatt, P., MacGinley, T., Choo, B., Reinforced concrete design to Eurocodes, CRC Press, USA, 2014

[20] Toniolo, G., Di Prisco, M., Reinforced concrete design to eurocode 2, Springer, Switzerland, 2017

[21] Issa, M.S., El-Abbasy, A.A., Examples oriented reinforced concrete text book according to ACI318, Dar Elmaarefa, Cairo, Egypt, 2019

[22] Al Hazmi, H.S.J., El-Abbasy, A.A., Abou Elmal, H.S., Applying Saudi Building Code (SBC 304) in teaching reinforced concrete courses in Jazan University, International Conference on Engineering Education (ICEE), Madinah, Kingdom of Saudi Arabia, 2011

[23] Nirusha, D.S., Prasad, R., Prediction of percentage of steel for singly and doubly reinforced beam sections using artificial neural network, Glob. J. Eng. Appl. Sci., 2011, 1: 127–129

[24] Yousif, S.T., ALsaffar, I.S., Ahmed, S.M., Optimum design of singly and doubly reinforced concrete rectangular beam sections: Artificial neural networks application, Iraqi J. Civ. Eng., 2010, 6: 1–19

[25] Panjehpour, P., Sorooshian, S., Deepak, T.J., The threshold for under-reinforced concrete sections proposed by ACI 318, EC 2 and BS 8110, Civ. Eng.

Archit., 2021, 9: 1754–1758. doi: 10.13189/cea.2021.090609

[26] El-Abbasy, A.A., Integrated interaction diagrams for sections subjected to axial force and bending moment according to the American Concrete Institute and the Saudi Building Code, Arab. J. Sci. Eng., 2021, 46: 4577–4592

[27] ASTM C39, Test method for compressive strength of cylindrical concrete specimens, ASTM International, USA, 2017. doi: 10.1520/C0039_C0039M-17B

[28] S.-E. CEN, Cement-Part 1: Composition, specifications and conformity criteria for common cements, European Commitee for Standarization, Brussels, 2011

[29] S.E. CEN, Methods of testing cement – Part 1: Determination of strength, Vol. 169, European Commitee for Standarization, Brussels, 2005, p. 36

[30] ASTM A572, Specification for high-strength low-alloy Columbium-Vanadium structural steel, ASTM International, USA, 2015. doi: 10.1520/A0572_A0572M-15

[31] ASTM C31, Practice for making and curing concrete test specimens in the field, ASTM International, USA, 2017. doi: 10.1520/C0031_C0031M-17

[32] ACI 308R-01 R08, Guide to curing concrete, American Concrete Institute, Farmington Hills, MI, USA, 2008

[33] Pauw, A., Static modulus of elasticity of concrete as affected by density, ACI J. Proc., 1960, 57(6): 679–683

[34] American Concrete Institute, Report on high-strength concrete (ACI 363R-10), ACI Committee 363, Farmington Hills, Michigan, USA, 2010

[35] Kaar, P.H., Hanson, N.W., Capell, H.T., Stress–strain characteristics of high-strength concrete, Spec. Publ., 1978, 55: 161–186

[36] Hognestad, E., Hanson, N.W., McHenry, D., Concrete stress distribution in ultimate strength design, In Journal Proceedings, 1955, pp. 455–480

[37] Popovics, S., A review of stress–strain relationships for concrete, In Journal Proceedings, 1970, pp. 243–248